



ELSEVIER

Available online at www.sciencedirect.com

SCIENCE @ DIRECT®

Solar Energy Materials
& Solar Cells

Solar Energy Materials & Solar Cells 83 (2004) 273–292

www.elsevier.com/locate/solmat

Organic photovoltaics: technology and market

Christoph J. Brabec*

Siemens AG, Corporate Technology, CT MMI, Paul-Gossen-Strasse 100, D-91052 Erlangen, Germany

Abstract

Organic photovoltaics has come into the international research focus during the past three years. Up to now main efforts have focused on the improvement of the solar conversion efficiency, and in recent efforts 5% white light efficiencies on the device level have been realized. Despite this in comparison to inorganic technologies low efficiency, organic photovoltaics is evaluated as one of the future key technologies opening up completely new applications and markets for photovoltaics. The key property which makes organic photovoltaics so attractive is the potential of reel to reel processing on low cost substrates with standard coating and printing processes. In this contribution we discuss the economical and technical production aspects for organic photovoltaics.

© 2004 Elsevier B.V. All rights reserved.

Keywords: Organic photovoltaics; Efficiency; Reel to reel processing

1. Introduction

Classical photovoltaics has an unfavourable cost structure compared to alternative renewable energy technologies; nevertheless, the continued high interest in this technology originates from the fact that photovoltaics is the only true portable and renewable source of energy available today. The essential cost-driving factor for the production of photovoltaic cells is the expensive investment into costly semiconductor processing technologies. Due to this the thought of photovoltaic elements based on thin plastic carriers, manufactured by printing and coating techniques from reel to reel, and packaged by lamination techniques is not only intriguing but highly attractive from a cost standpoint. In order to fulfil these requirements, high volume production technologies for large area coating must be

*Tel.: +49-9131-7-422-45; fax: +49-9131-7-324-69.

E-mail address: christoph.brabec@siemens.com (C.J. Brabec).

applied to a low cost material class. Solution processable organic and inorganic semiconductors have a high potential to fulfil these requirements. Flexible chemical tailoring allows the design of organic semiconductors with the desired properties, and printing or coating techniques like screen, inkjet, offset or flexo printing are being established for semiconducting polymers today, driven by display or general electronic demands. Altogether, organic photovoltaics has many attractive features, amongst them

- the potential to be *flexible and semitransparent*,
- potential to be manufactured in a *continuous printing process*,
- *large area* coating,
- *easy integration* in different devices,
- *significant cost reduction compared to* traditional solutions,
- substantial *ecological and economic advantages*.

These features are beneficial for commercialization, however, like its classical counterpart, organic photovoltaics has to fulfil the basic requirements for renewable energy production. In the energy market the competitive position of every solar technology is mainly determined by the factors efficiency, lifetime and costs (per W_p). The potential of organic photovoltaic has to be judged by these key figures as well. We believe that if organic photovoltaics is able to realize a certain technological profile, than there will be substantial freedom for commercialization. Fig. 1 summarizes the restrictions within which organic photovoltaics can be commercialized. The important message of this figure is that successful commercialization can be realized only if all three technology driving aspects are fulfilled at the same time. A product development succeeding in only two aspects like, e.g. competitive costs and reasonable efficiency, will only be able to address niche markets unless the third parameter, in that case, life time, is also optimized.

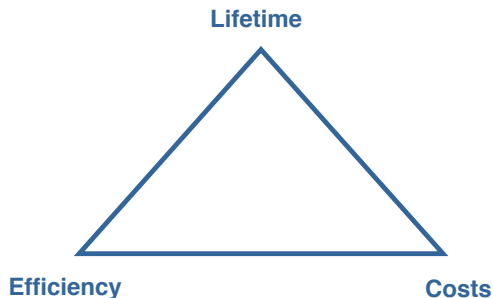


Fig. 1. The critical triangle for photovoltaics. Organic solar cells have to fulfil all requirements simultaneously, lifetime, efficiency and costs; otherwise they will be limited to a niche market. Additional criteria like semi-transparency, flexibility or very short *break even times* are beneficial, but cannot make up for a significant deficiency in one of the triangle's corners.

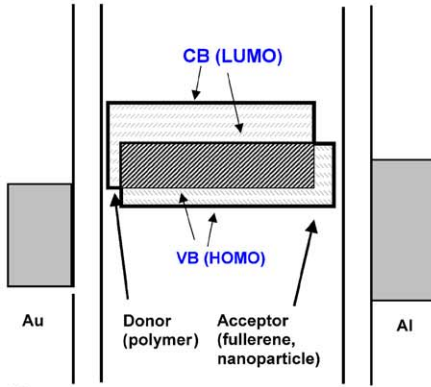
2. Organic photovoltaics—concept

Most organic semiconductors are intrinsic semiconductors and the primary excitation is a Coulomb bound exciton. Photovoltaic cells made from single organic semiconductors therefore achieve tiny power conversion efficiencies and low incident-photon-to-current or external quantum efficiencies (EQE). A high EQE does not guarantee good photovoltaic energy conversion, but it is a prerequisite. For inorganic photovoltaic devices routinely EQEs approaching 100% are achieved. For organic photovoltaic devices comprising a single polymeric semiconductor layer EQEs are typical below 1%. A solution was only found in 1995, when several groups independently showed that the EQE could be enhanced by several orders of magnitude upon blending two materials with relative preferences for positive and negative charges [1–3]. The difference in electron affinities creates a driving force at the interface between the two materials that is strong enough to split photogenerated excitons. By blending materials on a nanostructured scale (about 10 nm), the interface is distributed throughout the device. Hence, all photogenerated excitons are likely to find an interface and split before recombining if the charge transfer is significantly faster than competing recombination channels, either radiatively or non-radiatively. The separated charges must then travel through the appropriate material toward the contacts. The concept of blending p-type semiconductors with n-type semiconductors has become popular under the name bulk heterojunction composites [4].

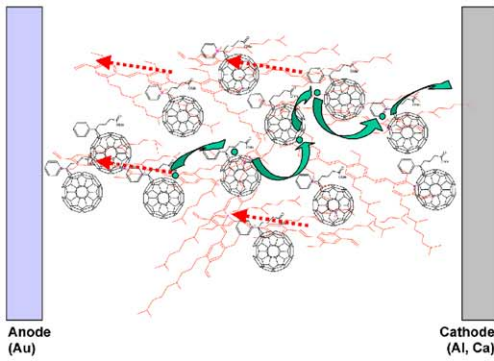
The EQE represents that fraction of photoexcitations that survive both charge separation and transport processes. Using the bulk heterojunction concept the EQE has been increased from 29% [3] to 50% [5] and recently an EQE of 80% was reported [6]. These impressively high values have been obtained for blends of conjugated polymers with fullerenes.

Solution processing may qualify polymeric photovoltaics as an alternative renewable energy source. Unfortunately, overall power conversion efficiencies under the normalized solar conditions are low. Highest efficiencies of only about 3.5% have been reported so far [7–9], and just recently the critical 5% efficiency benchmark has been overcome [10]. One of the main reasons for this still somehow disappointingly low power efficiency despite the high EQE is the spectral mismatch of the organic absorbers to the solar spectrum. Most of the organic semiconductors investigated today absorb in the visible range, while the sun has its maximum photon density at around 700 nm. Another problem is a certain intrinsic limited durability of organic compounds: when electrons are excited to higher orbitals, anti-binding states arise and the probability for decomposition of the compound increases. This is particularly true for n-type semiconductors.

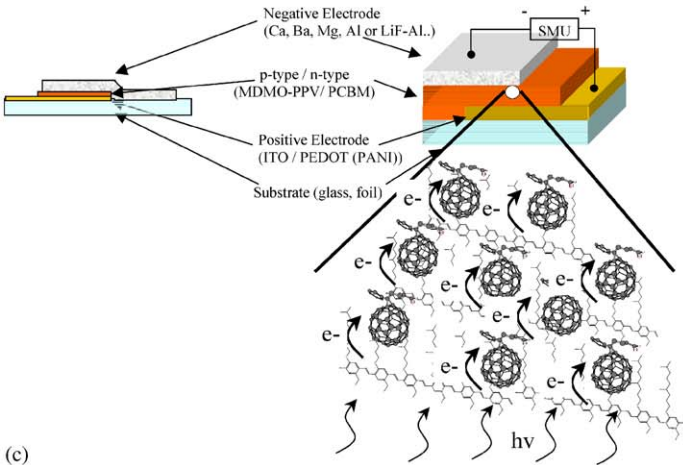
Finally, effective light harvesting in a blend photovoltaic device demands efficient charge separation and transport. First, the energy bands of the two materials have to cascade in order to guarantee charge generation after photoexcitation (Fig. 2a). Second, each material must provide a continuous path for the transport of separated charge to the contacts (Fig. 2b). This demands a highly complex morphology between the two compounds with interconnected domains in the nanometer scale to



(a)



(b)



(c)

prevent trapping and more ordered regions in the 100 nm scale to guarantee efficient transport channels.

3. Efficiency

Efficiency is the essential parameter for solar cells with respect to energy production and cost. The overall efficiency η_{eff} of a solar cell is calculated by the following formula:

$$\eta_{\text{eff}} = V_{\text{oc}} * I_{\text{sc}} * \text{FF} / I_{\text{light}}, \quad (1)$$

where V_{oc} is the open circuit voltage, typically measured in V , I_{sc} the short circuit current density in A/m^2 , FF the fill factor and I_{light} the incident solar radiation in W/m^2 . More detailed, the AM1.5 conversion power efficiency $\eta_{\text{AM1.5}}$ of the photovoltaic devices measured with a solar simulator is given by

$$\eta_{\text{AM1.5}} = \frac{P_{\text{out}}}{P_{\text{in}}} M = \text{FF} \frac{V_{\text{oc}} J_{\text{sc}}}{P_{\text{in}}} M, \quad (2)$$

where P_{out} is the output electrical power of the device under illumination, P_{in} is the light intensity incident on the device as measured by a calibrated reference cell. M is the spectral mismatch factor that accounts for deviations in the spectral output of the solar simulator with respect to the standard AM1.5 spectrum and deviations in the spectral response of the device under measure with respect to that of the reference cell [11]. For measurements with solar simulators utilizing a metal-halogenide lamp, the mismatch factor is determined with $M \sim 0.76$ while a solar simulator utilizing a Xenon lamp typically has a mismatch factor of $M \sim 0.9$ under $P_{\text{in}} = 80 \text{ mW}/\text{cm}^2$.

In the following we will discuss and summarize results for organic bulk-heterojunction devices. For the devices discussed in this chapter, poly(2-methoxy-5-(3',7'-dimethyloctyloxy)-1,4-phenylene-vinylene) (MDMO-PPV) or alkyl polythiophenes (P3AT) as electron donor and p-type semiconductor were used, while the electron acceptor was [6,6]-Phenyl C_{60} -butyric acid methyl ester (PCBM). MDMO-PPV, P3AT and PCBM are prototype organic semiconductors, which fulfil the basic

←

Fig. 2. (a) Charge generation and transport in bulk heterojunction solar cells. Photon harvesting in a bulk heterojunction photovoltaic device demands efficient charge separation (a) and transport (b). (a) The energy bands of the two materials have to arrange in order to support charge transfer after photoexcitation. Charge separation can occur if conduction bands (or LUMO), respectively, the valence bands (or HOMO) of the acceptor and the donor are misaligned in such a way, that charge transfer from the donor to the acceptor becomes energetically favourable. (b) Schematic drawing for charge transport in bulk heterojunction composites. Fullerenes stand respectively for acceptors, organic or inorganic nanoparticles. Each component of the bulk heterojunction composite must provide a continuous path for the transport of separated charge to the contacts. Transport paths are indicated by dashed lines for positive carriers and by full arrows for negative carriers. Isolated domains can trap charges, whereas linear, ordered regions can act as efficient transport channels. (c) Schematic drawing of the thin film solar cells. The organic layer is sandwiched between two metallic electrodes. The thickness of the photoactive layer is only a few 100 nm.

requirements for organic photovoltaics. Both semiconductors can be produced with high purity and a low defect density, they are truly intrinsic (typically with a carrier concentration much less than 10^{15} cm^{-3}), and show satisfactory solubility in a large number of organic solvents.

The cross-section of bulk-heterojunction solar cells is depicted in Fig. 2c. Indium doped tin oxide (ITO) glasses are typically used as semitransparent substrates with a transmissivity of $\sim 90\%$ in the visible range and a conductivity of $\sim 20 \Omega/\text{square}$. Poly(ethylene dioxythiophene) doped with polystyrene sulphonic acid (PEDOT:PSS, Bayer AG) is spin-coated on top of the ITO from a water solution, giving a conductive ($\sim 10^{-3} \text{ S/cm}$) layer which prevents shorts and allows to increase the shunt resistivity of the thin film devices. The photoactive layer consisting of polymer/fullerene composites again is coated on top of the PEDOT to a thickness of $\sim 100 \text{ nm}$ from solution.

The negative electrode (cathode, typically, Ca/Al, Ba/Al or LiF/Al) is thermally deposited through a shadow mask. The geometrical overlap between the positive electrode and the negative electrode defines the active area. In the following strategies and concepts to optimize the power efficiency of polymeric solar cells based upon bulk heterojunctions are discussed.

The open circuit voltage: A highly interesting phenomenon in the bulk heterojunction cells based on organic (polymeric) semiconductors is the observation of unusual high open circuit voltages. Before discussing the observations in bulk heterojunction solar cells, the findings for pristine conjugated polymer PV elements are briefly reviewed.

For single layer polymer PV elements, produced by spin casting from alkoxy PPV solutions, a consistent picture is found for the experimental observation and an explanation of the open circuit voltage is given. For devices with high purity ($N_d \ll 10^{17} \text{ cm}^{-3}$), it is argued that a single layer polymer device works as a Metal–Insulator–Metal (MIM) diode [12]. The experimentally observed V_{oc} of bulk heterojunction cells cannot be explained by the MIM picture alone. For typical devices, based on ITO/conj. Polymer–fullerene/Al, V_{oc} in the range of 800 mV and higher can be observed for several polymer/fullerene mixtures, in contrast to the 400 mV expected from the MIM picture. The chapter on the V_{oc} will discuss and explain the origin of the open circuit voltage in plastic solar cells.

The fill factor: The fill factor of solar cells as determined by

$$FF = I_{mpp}^* V_{mpp} / I_{sc}^* V_{oc} \quad (3)$$

with I_{mpp} and V_{mpp} as the current and the voltage in the maximum power point of the I/V curve in the 4th quadrant, reflects the diode properties of the solar cells.

In general, a large serial resistance as well as a too small parallel resistance (shunt) tend to reduce the FF. Strategies to reduce the serial resistivity by improving the quality of the ohmic contact will be discussed.

The short circuit current: A key parameter for the efficient charge collection of plastic solar cells is the hole and the electron mobility of the interpenetrating networks and the lifetime of the carriers within this network. The interplay of the

network quality, the mobility and their impact on the short circuit current will be discussed at the hand of a simple model in this chapter.

3.1. The open circuit voltage V_{oc}

Solar cells are semiconductors under illumination, where the absorption of light leads to a generation of carriers. After the carrier generation, the excess energy of the carriers (in the case of photons with energies larger than the bandgap of the carrier) will be lost by interaction with the lattice (phonons). After this thermalization process the carriers are in equilibrium in their bands before they are lost by recombination. The carrier densities are given by two Fermi distributions, one for the electrons and one for the holes. This concept is strictly valid for the semiconductor under illumination. The electron and the hole densities are then given by

$$n_e = N_C \exp\left(-\frac{\varepsilon_C - \varepsilon_{F,C}}{kT}\right), \quad n_h = N_V \exp\left(-\frac{\varepsilon_{F,V} - \varepsilon_V}{kT}\right), \quad (4)$$

N_C and N_V are the effective densities of states of the conduction and the valence band; ε_C , ε_V , $\varepsilon_{F,C}$ and $\varepsilon_{F,V}$ are the conduction band energy, the valence band energy, the electron quasi Fermi energy and the hole quasi Fermi energy. The product $n_e n_h$ becomes

$$n_e n_h = n_i^2 \exp\left(\frac{\varepsilon_{F,C} - \varepsilon_{F,V}}{kT}\right). \quad (5)$$

This difference between the two quasi Fermi levels will therefore be an upper limit for the open circuit voltage. For thin film photovoltaic devices the built in potential is an essential parameter for several reasons, influencing charge dissociation, charge transport and charge collection. A generally accepted estimation for the built-in potential is given by the open circuit voltage V_{oc} , which underestimates the built-in potential at room temperature and converges to the correct value at low temperatures. Therefore, the question of the built-in potential is directly related to an extensively discussed phenomenon, the origin of the open circuit voltage V_{oc} . Mixing fullerenes with conjugated polymers into a composite active layer completely modifies the nature of the thin film devices compared to those made with conjugated polymers alone [13,14] and hence the V_{oc} of the corresponding solar cells. Three different variations of the devices are introduced in order to analyse the V_{oc} of bulk heterojunction cells:

3.1.1. Variation of top electrode materials

In order to systematically investigate the critical parameters influencing the built-in potential in conjugated polymer/fullerene bulk heterojunction solar cells, a series of highly soluble fullerene derivatives with varying acceptor strength (i.e. first reduction potential) are tested and the open circuit voltage of the corresponding devices as a function of the acceptor strength can be analysed. These fullerene derivatives, methanofullerene PCBM, an azafulleroid and a ketolactam

quasifullerene, show a variation of almost 200 mV in their first reduction potential. Additionally, cells made with [60]fullerene (C_{60}) are compared. The highest and the lowest averaged open circuit voltages are observed for the PCBM containing cells and for the ketolactam containing cells with 760 and 560 mV, respectively [15].

3.1.2. Variation of top electrode materials

PCBM is chosen as reference electron acceptor to investigate the influence of top (negative) electrodes with different work functions on the built-in potential of conjugated polymer/fullerene bulk-heterojunction plastic solar cells. Devices with Ca ($\phi_{Me} = 2.87$ eV), (Al $\phi_{Me} = 4.28$ eV), (Ag $\phi_{Me} = 4.26$ eV) and (Au $\phi_{Me} = 5.1$ eV) [16] as negative electrodes have been investigated. A total variation of less than 200 mV of the V_{oc} is observed for a variation of the negative electrode work function by more than 2.2 eV. For the devices with an Au electrode, V_{oc} is found to be slightly lower than the average value, but still as high as 650 mV. The Ca devices exhibit a V_{oc} of 814 mV [15].

3.1.3. Variation of bottom electrode

A material commonly chosen as the polymeric p-type contact (anode) is poly(3,4-ethylenedioxythiophene) (PEDOT) doped with poly(styrenesulfonate) (PSS). It has been recently demonstrated that its work-function (ϕ_w) can be conveniently altered electrochemically [17]. This technique has been used in order to systematically study the influence of V_{bi} in ITO/PEDOT/photoactive donor–acceptor blend/Al devices. PEDOT was polymerized electrochemically on indium tin oxide (ITO) as a transparent electrode. In a second step it was electrochemically adjusted *ex situ* to the desired equilibrium potential E_{eq} . A blend of the soluble fullerene derivative [6,6]-phenyl-C61-butyric acid-methylester (PCBM; acceptor) and MDMO-PPV (donor) was spin-casted as the photoactive material, and finally the aluminum contact was evaporated.

Fig. 3 shows the dependency of V_{bi}^* on E_{eq} , i.e. the work function of PEDOT. In perfect agreement with earlier PV studies on OLED devices using pristine MDMO-PPV, a linear dependence with a slope of 0.8 is found, indicating that the ϕ_w of the PEDOT layer is not pinned to any of the energy levels present within the active layer blend. The PV results deviated from the linear dependency (Fig. 3a) whenever E_{eq} of the PEDOT anode approached or even exceeded the oxidation potential E_{ox} of MDMO-PPV as determined by cyclic voltammetry in solution (Fig. 3c). We attribute this to redox chemistry between the MDMO-PPV and the highly oxidized PEDOT layer (see below). Because of these redox reactions, the range $E_{eq} > E_{ox}$ is “forbidden” (shaded area in Fig. 3a). On the other hand, passing the reduction potential of PCBM (Fig. 3d) does not seem to harm V_{bi}^* . This finding can be explained in terms of missing redox states for completely dedoped (neutral) PEDOT (compare Fig. 3b) and, therefore, the absence of a sufficient number of counter ions, which are necessary to compensate redox reactions across the interface. We point out, that exact correlations between the redox potentials determined in solution (Figs. 3c and d) and the situation in a real device is not possible. However,

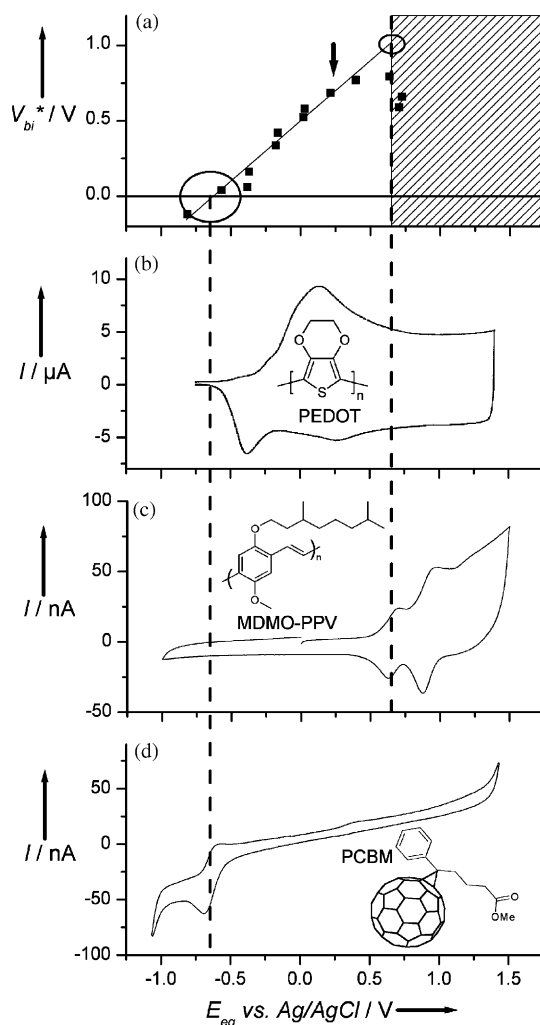


Fig. 3. Comparison of OSC device performance with electrochemical properties of involved compounds. (a) Built-in potential V_{bi}^* in devices PEDOT(E_{eq})/MDMO-PPV:PCBM/Al as a function of the pre-adjusted E_{eq} of the PEDOT layer. The shaded area indicates the "forbidden" potential range, in which PEDOT is able to oxidize MDMO-PPV (see "doped" OSCs). The arrow indicates the commercial PEDOT. (b) Cyclic voltammogram of a PEDOT-film atop the Pt work electrode in acetonitrile with tetrabutylammonium hexafluorophosphate (TBAPF₆, 0.1 M). The scan rate was $v=10$ mV/s. (c) Cyclic voltammogram of MDMO-PPV in methylene chloride with TBAPF₆ (0.1 M), $v=100$ mV/s. The right-hand vertical dashed line indicates the first oxidation potential (defining the beginning of "forbidden" potential range). (d) Cyclic voltammogram of PCBM in methylene chloride with TBAPF₆ (0.1 M), $v=100$ mV/s. The left-handed vertical dashed line indicates the first reduction potential.

electrochemical investigations of solid films of the respective materials will be similarly problematic due to slow electron transfer kinetics, generally leading to scan-rate dependent overpotentials.

3.1.4. V_{oc} discussion

The experimental results on the variation of the acceptor strength and on the variation of the top and bottom electrode work function indicate that organic solar cells have two different interfaces. A variation of the workfunction of the positive electrode (ITO/PEDOT) linearly influences the open circuit voltage of the solar cell, with a scaling factor of ~ 0.8 . Contrarily, variation of the workfunction of the negative electrode results in a weak variation of the open circuit with a scaling factor of ~ 0.1 . A variation of the valence band of the n-type semiconductor results in a change of the open circuit voltage with a scaling factor ~ 1 . Summarizing, we find a strong coupling of the V_{oc} to the conduction band of the n-type semiconductor and to the workfunction of the positive contact, together with a weak coupling to the work function of the negative contact.

The fact that a “zero-built-in-field” solar cell can be realized when the work function of the PEDOT equals the reduction potential of PCBM demonstrates that the pinning of the cathode (here Al) occurs exactly at the LUMO level of the PCBM acceptor. No pinning of the PEDOT energy levels to the PCBM LUMO level is observed unlike demonstrated for the metal cathode. However, the latter is a result of the thermal evaporation process. The negative electrode insensitive voltage behaviour is specific for the negative electrode in polymer/fullerene bulk heterojunction solar cells and is discussed in terms of Fermi level pinning between the negative metal electrode and the fullerene reduction potential via charged interfacial states.

From the results presented above, the following equation for the open circuit voltage is proposed:

$$V_{oc} = (S_4 * A_{ox} + S_3 * (\phi_{M1} - A_{ox})) - S_1 * E_{red(A)} - S_2 * (\phi_{M2} - E_{red(A)}) + C. \quad (6)$$

Here $E_{red}(\text{fullerene})$ is the reduction potential of the acceptor (fullerene derivative), A_{ox} the oxidation potential of the donor (conjugated polymer) and S_1, S_2, S_3 and S_4 are the correlation factors between the V_{oc} and the fullerene conduction band, the negative electrode’s work function ϕ_{M2} , the positive electrode’s work function ϕ_{M1} and polymer’s valence band as discussed above. Since the parameter S_2 is found to be sufficiently small ($S_2 < 0.1$), and S_1 as well as S_3 are close to unity, Eq. (6) can be further simplified leading to:

$$V_{oc} = \phi_{M1} - E_{red(A)} \text{ only if } A_{ox} > \phi_{M1},$$

$$V_{oc} = A_{ox} - E_{red(A)} \text{ only if } A_{ox} < \phi_{M1}, \quad (7a, b)$$

Please note, that Eq. (7a) strictly is valid if the work function of the positive electrode is smaller than the oxidation potential of the donor (p-type semiconductor), i.e. $A_{ox} > \phi_{M1}$. In the reverse case, $A_{ox} < \phi_{M1}$, Eq. (7b) is correct.

3.2. The FF

For practical solar cells, the ideal equivalent circuit will be modified to include the series resistance from the ohmic loss in the two electrodes and the shunt resistance

from leakage currents (Fig. 4). The diode current for a realistic circuit is then given by

$$\ln((I(V) + I_{sc})/I_0 - (V - IR_s)/I_0 R_p + 1) = q(V - IR_s)/nkT, \quad (8)$$

where I_0 , R_s , R_p , n and q/kT are the saturation current density, the serial and parallel resistivity, the diode ideality factor and the temperature potential (25 mV at room temperature), respectively. The influence of R_s and R_p on the fill factor are obvious, more difficult is the influence of I_0 and n via modification of the dark diode contributions on the fill factor.

Recent progress in the development of electrodes for bulk heterojunction solar cells [7] includes a strategy of incorporating a small amount of LiF at the interface between the photoactive layer and the aluminum cathode. This technique has previously been used to enhance the performance of organic light-emitting diodes for devices fabricated by solution casting of polymers [18,19]. In this chapter, the performance of the bulk-heterojunction photovoltaic devices with respect to the FF is studied as a function of contact quality. Insertion of thin layers of LiF (< 15 Å) are discussed to increase both the open circuit voltage and the fill factor of the device, yielding an increased power conversion efficiency.

A strong increase in the forward current and in the FF is observed for conjugated polymer/fullerene bulk heterojunction solar cells (MDMO-PPV/PCBM) upon reducing the serial resistivity across the contact. This is performed by insertion of a thin layer of LiF between the organic semiconductor layer and the Al electrode (negative electrode of the solar cell).

A box plot diagram is chosen to present the results from current/voltage (I/V) measurements for the FF (Fig. 5a) and the V_{oc} (Fig. 5b). At least 6 different devices are evaluated for each LiF thickness which is varied between 0 and 15 Å. Upon insertion of only 3 Å of LiF, the FF already increased by app. 20% compared to otherwise identical reference devices with a pristine Al electrode. Together with an I_{sc} of 5.25 mA/cm², an V_{oc} of 825 mV, the white light power conversion efficiency under

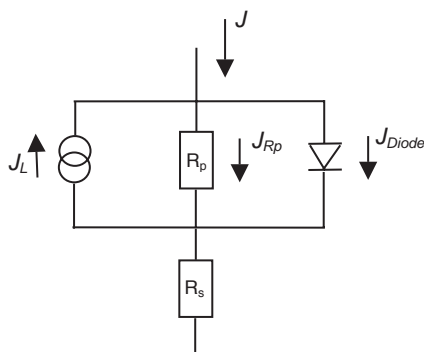


Fig. 4. Replacement circuit for organic solar cells. Replacement circuit for a solar cell. The parallel resistivity R_p resembles all shunts while the serial resistivity resembles the bulk resistivity of the active area, the contact resistivity and the circuit resistivity.

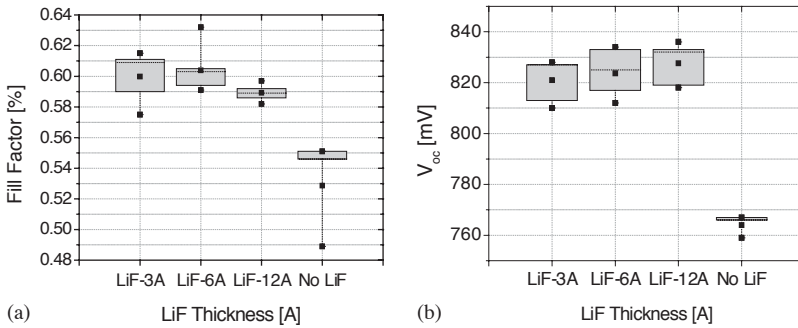


Fig. 5. Characteristics of typical MDMO-PPV/PCBM solar cells with a LiF/Al electrode of various LiF thickness (v : 3 Å, λ : 6 Å, σ : 12 Å) compared to the performance of a MDMO-PPV/PCBM solar cell with a pristine Al electrode. (a) and (b) are box plots with the statistics of the FF and the V_{oc} from 6 separate solar cells. LiF or SiO_x were thermally deposited with a rate of $1\text{--}2 \text{ \AA}/\text{min}$ from a tungsten boat in a vacuum system with a base pressure of 10^{-4} Pa. We emphasize that for thickness values on the order of ~ 1 nm the LiF/ SiO_x is not a continuous, fully covering layer, but instead consists of island clusters on the surface of the photoactive layer. Slow evaporation conditions are essential for more homogenous distribution of the LiF on the organic surface. The nominal thickness values given here represent an average value across the surface of the substrate. The metal electrode (either aluminum or gold) was thermally deposited with a thickness of 80 nm.

$800 \text{ W}/\text{m}^2$ at 50°C is calculated to be 3.3% (please note, that this is a white light efficiency which is not corrected by a spectral mismatch factor M).

Further increase of the layer thickness (up to 9 Å) does not change the average value of the FF, but narrows considerably the distribution of the FF of the single devices. At a LiF layer thickness of already 12 Å a slight decrease of the FF is observed and at a layer thickness exceeding 20 Å the beneficial influence of the LiF layer on the FF is lost due to the high resistivity of the LiF layer.

A numerical fitting analysis was applied to the I/V curves. The current equation of an ideal Shottky diode [20] is rewritten from Eq. (8) and numerically fitted to the experimental data by a recursive algorithm, allowing to extract the diode parameters. For all diodes excellent fits can be generated with this one diode model. The calculated values for the serial resistivity R_s and the shunt resistivity R_p are also summarized in Ref. [7]. While there is little or no change in the shunt resistivity for all of the diodes, the serial resistivity of the diodes is lowered by a factor of 3–4 upon insertion of a thin LiF layer, independent of the evaporated metal. This lowering of the serial resistivity is responsible for the increase of the FF due to formation of a better ohmic contact as discussed previously.

The precise mechanism of LiF on the interface between metals and organic semiconductors is still under discussion. It is interesting to note, that, differently to OLEDs, Cs and K related salts (CsF, KBr) do not positively influence the solar cell performance [21]. Nevertheless, LiF/Al cathodes are a proper electrode for high fill factors.

3.3. The ISC

The interpenetrating network in bulk heterojunction solar cells helps to overcome the limitations of bilayer systems [22] with low mobility materials. However, less is known on the nanometer morphology of an interpenetrating network and on the optimum density of donor/acceptor interfacial contacts that facilitate both, the photoinduced creation of mobile charge carriers as well as transport of the carriers to the electrodes. In this chapter the importance of the network morphology and the effect of the single component's morphology in the blends on the I_{sc} will be discussed. Structuring of the blend to form a more intimate mixture that contains less phase-segregation of the methanofullerene species, thus simultaneously increasing the degree of interactions between conjugated polymer chains is straightforward. Improving the mobility of the polymeric semiconductor (obviously the component with the lower mobility in the blend as discussed in the previous chapter) is another important step towards I_{sc} improvement.

Once this metastable charge-separated state is formed, the free charges are transported through the device through diffusion and drift processes. The latter is induced by using top and bottom layer electrodes that have different work-functions, thus providing a built-in electric field over the active layer [13]. In the active layer of the device, holes are transported through the conjugated polymer matrix, and electrons are transported by hopping between fullerene molecules. Importantly, these two different charge transport processes do not interfere with each other. Field-effect mobility measurements have shown that mixing of a methanofullerene into a conjugated polymer matrix (using the same materials and doping level as in the devices presented in this work) does not or only negligibly reduce the hole mobility [23,24].

Fig. 6 shows AFM images of the surfaces of MDMO-PPV:PCBM blend films spin-coated using either toluene or chlorobenzene. The images show clearly different surface morphologies. The surface of the toluene-cast film contains structures with horizontal dimensions on the order of $0.5\ \mu\text{m}$. Since the horizontal dimensions of these features are much larger than the thickness of the film (100 nm), it can be concluded that the morphology seen on the surface is representative of that throughout the bulk. Since such features are not observed in films of pristine MDMO-PPV spin-coated from toluene, they are assigned to be phase-segregated regions that contain higher concentrations of fullerenes. In contrast, the chlorobenzene-cast film contains structures with horizontal dimensions on the order of only $0.1\ \mu\text{m}$. This indicates a much more uniform mixing of the constituents. Furthermore, the toluene-cast film has height variations on the order of 10 nm, whereas the chlorobenzene-cast film is extremely smooth, with height variations on the order of 1 nm. This contrast in film morphologies is mainly attributed to the fact that the solubility of PCBM in chlorobenzene is more than twice that in toluene, however, also the solubility of the polymer in these two solvent changes.

Results from AFM studies are supported by light scattering data to measure solutions of MDMO-PPV in toluene versus chlorobenzene. MDMO-PPV typically has a molar mass distribution (M_w) of $\sim 10^6$ mol/g and a polydispersity below 2. The

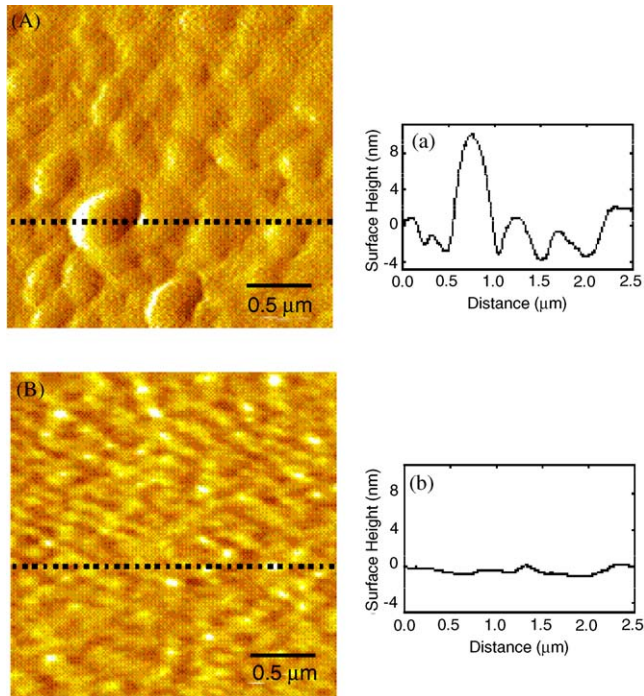


Fig. 6. AFM images (acquired in the tapping mode) showing the surface morphology of MDMO-PPV : PCBM (1:4 by wt.) blend films with a thickness of approximately 100 nm and the corresponding cross sections. (A) Film spin-coated from a toluene solution. (B) Film spin-coated from a chlorobenzene solution. The images show the first derivative of the actual surface heights. The cross-sections of the true surface heights for the films were taken horizontally from the points indicated by the arrow.

particle size distribution in the MDMO-PPV solutions can be analysed by means of light scattering measurements [25]. This technique allows determining the particle size (PS) in solutions, which can be expressed as a number distribution or as a volume distribution. It was shown that in toluene, the number PS develops upon dilution from 35 over 6 nm to more than 6 μm [25]. The volume PS increases from 2.2 μm over 3.2 μm to > 6 μm . At the highest concentration (0.25%), 2 fractions can be distinguished from which the smaller decreases further in the first dilution and completely vanishes at the lowest concentration (0.0625%). The latter is indicative for a true solution. At the concentration of 0.25%, toluene provides at least a partial solubility for MDMO-PPV. In this case, vacancies are created within the polymer coil that can be occupied by toluene molecules, in this way possibly hindering interchain interactions. In chlorobenzene, the number PS decreases from 66 down to 8 nm upon dilution. At the concentration of 0.25%, there are four (partially overlapping) PS fractions, which are reduced to just one fraction at medium concentration. At the lowest concentration, a new fraction develops around a PS of 5.5 μm . These data indicate that the chlorobenzene solutions with high and medium

concentrations form a colloidal system, rather than a solution. It is likely to assume that in these colloids chromophore aggregation and thus interchain interactions are promoted. As the degree of aggregation is known to be preserved throughout the spin-casting process, we can conclude that the solution aggregation will also be mirrored in the thin film systems.

To compare the impact of these different morphologies on the photovoltaic device performance, devices were fabricated in an identical manner except for the choice of solvent (either toluene or chlorobenzene) used for spin-coating the active layer (MDMO-PPV : PCBM, 1:4 by wt.). Characterization of the devices is performed under illumination by a AM 1.5 corrected solar simulator.

A plot of the current density versus voltage for the two devices is shown in Fig. 7. The open-circuit voltages of the cells are identical (0.82 V). However, the chlorobenzene-based device exhibits a more than 2-fold increase in the short-circuit current density as compared to the toluene-based device (5.25 versus 2.33 mA/cm²). As shown in Fig. 8a, the optical transmission spectra of the active layer films are nearly identical, except for a small red-shift in the MDMO-PPV absorption (425–575 nm) in the chlorobenzene-cast film, as expected for the case of increased interchain interactions. Thus, the chlorobenzene-based device is much more efficient at converting photons to electrons. This is explicitly demonstrated in Fig. 8b in the plot of external quantum efficiency, or incident photon to converted electron (IPCE) ratio, as a function of wavelength. The fill factor also increases (0.50 versus 0.61) upon changing the solvent from toluene to chlorobenzene. The increased short-circuit current density and fill factor due to the improved morphology yield a nearly 3-fold increase in the AM1.5 power conversion efficiency (0.9% versus 2.5%). Such a strong influence of the morphology on the performance of bulk

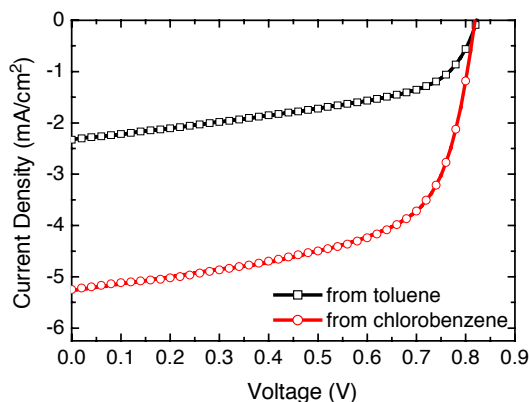


Fig. 7. Characteristics for devices with an active layer that is spin-coated from a toluene solution (open squares): $J_{sc} = 2.33 \text{ mA/cm}^2$, $V_{oc} = 0.82 \text{ V}$, $FF = 0.50$, $\eta_{AM1.5} = 0.9\%$, and from a chlorobenzene solution (open circles): $J_{sc} = 5.25 \text{ mA/cm}^2$, $V_{oc} = 0.82 \text{ V}$, $FF = 0.61$, $\eta_{AM1.5} = 2.5\%$. Data is for devices illuminated with an intensity of 80 mW/cm^2 with an AM1.5 spectral mismatch factor of 0.753. The temperature of the samples during measurement was 50°C .

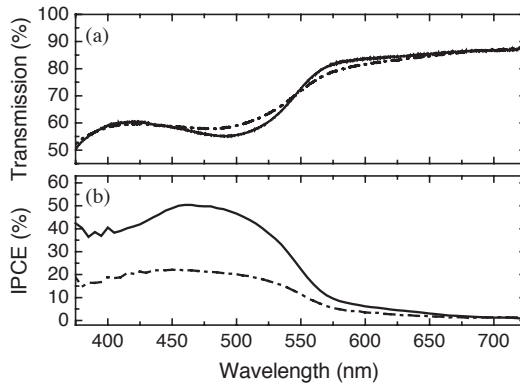


Fig. 8. (a) Optical absorption spectra of 100 nm thick MDMO-PPV : PCBM (1:4 by wt.) films spin-coated onto glass substrates from either toluene (dash dotted line) or chlorobenzene (solid line) solutions. (b) IPCE spectra for photovoltaic devices using these films as the active layer.

heterojunction solar cells has been observed for a series of materials and material combinations.

It is generally accepted that charge transport along one polymer chain is a fast process. However, interchain transport relies on the hopping process, and measurements of charge carrier mobilities in films of MEH-PPV typically yield values four–five orders of magnitude lower than this. For fullerenes the situation is only slightly different. The transport of charges between the single fullerenes is the mobility determining step. A close packing of the fullerenes is a necessary prerequisite for good charge transport performance. Consequently, putting together p- and n-type semiconductors with the highest mobility should result in high performance with respect to efficiency. This is now demonstrated for another prototype polymer, a poly(alkyl thiophene).

Fig. 9a shows a typical I/V curve of a P3HT/PCBM based bulk heterojunction device with $\sim 4\%$. More interesting than the power efficiency are, in this case, the external and internal quantum efficiencies. Fig. 9b shows the typical EQE of P3HT/PCBM bulk heterojunction solar cells. A peak value of 76% is observed at 550 nm for a 350 nm thick device, one of the highest reported values for polymer based solar cells. Correction for temperature yields even higher values, an EQE of 80% at 70°C. While this is certainly an impressively high value, it is even more interesting to analyse, whether optical losses can explain the residual loss of 20%. The optical loss in the substrate of the bulk heterojunction device was analysed by absorption measurements in transmission geometry [6]. Absorption measurements on glass/ITO/PEDOT substrates revealed absorption losses of up to 13% under normal incidence at 550 nm. In order to determine the internal quantum efficiency, absorption measurements in reflection geometry, utilizing an integrating sphere, were done. At 550 nm, nearly 90% of the incident photons are absorbed by the device. The IQE, calculated as the fraction of electrons versus absorbed photons is

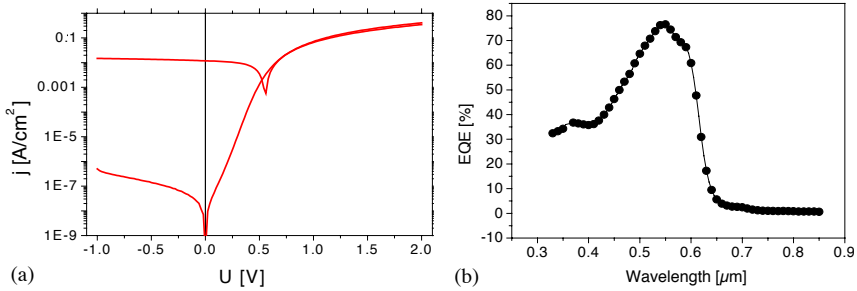


Fig. 9. Performance of P3HT/PCBM solar cells. (a) Dark and illuminated I/V characteristics of a typical polymer–fullerene bulk heterojunction solar cell with an efficiency of 3.85%, measured at 25°C and illuminated with 1 sun from a solar simulator. The short circuit current density I_{sc} is as high as $15 \text{ mA}/\text{cm}^2$. However, losses in the fill factor FF and the open circuit voltage are limiting efficiencies to the 4% level. Once these deficiencies are overcome, a power efficiency of $\sim 7\%$ is possible for this material combination. (b) Typical spectral photocurrent density of a polymer–fullerene bulk heterojunction device. The external quantum efficiency reaches the 80% level, the internal quantum efficiency (not shown here) is close to 100%. The spectral photocurrent rises at 650 nm, i.e. the bandgap of the absorber (1.9 eV).

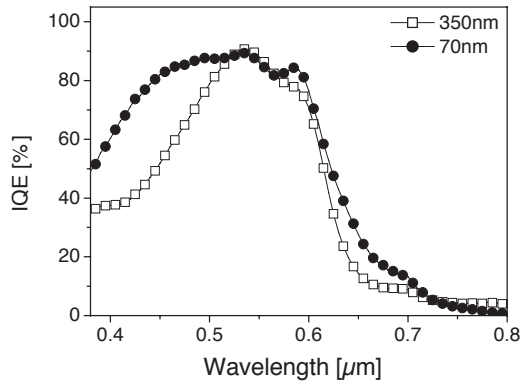


Fig. 10. Internal quantum efficiency (IQE) of the devices with an active layer thickness of 350 nm (hollow squares) and of 70 nm (full circles), as calculated from the ratio of EQE/absorbed photons.

plotted in Fig. 10. In the red spectral region, a peak maximum of 94% at 530 nm is observed at 25°C . Taking into account the positive temperature coefficient, the IQE at 70°C is expected to be $\sim 98\%$. Thus, the quantum efficiencies for charge generation and charge collection are both close to 100% at the peak wavelength.

EQE values around 80% for devices without reflection coatings or light trapping are an impressive demonstration that bulk heterojunction solar cells can reach high efficiency values. However, taking into account the performance of the device presented in Fig. 9b, the high EQE value not necessarily mirrors in high power efficiencies. Therefore, the question on the efficiency limitations for polymer based solar cells arises. From the EQE data it is already clear, that the lower mobility of

organic semiconductors compared to inorganic solar cells is not limiting the device performance [26,27]. The V_{oc} analysis revealed that open circuit voltages close to the theoretical limit for the materials can be reached. Certainly, fullerenes introduce a significant loss due to their too low reduction potential, approximately a factor of 2 compared to polymeric acceptors.

A detailed analysis of devices similar to the one shown in Fig. 9a, showed that used semiconductors have the potential to reach power efficiencies exceeding 7%, [9,10]. Organic solar cells with such high efficiencies will be demonstrated within the next 1–2 years. Once the high V_{oc} losses due to the fullerenes are overcome, efficiencies of 10% will be reached. Even higher efficiencies will demand novel materials with lower bandgaps and improved I_{sc} .

4. Costs

Since the encouraging development of polymer optoelectronic materials in the last few years has led to first commercial applications and products (OLED and PLED displays), the discussion of suitable production technologies becomes increasingly important. Up to now, mainly production technologies from traditional silicon microelectronics are used for the assembly of new polymer optoelectronic devices. However, the full advantage of polymer optoelectronic materials will only be exploited with very different processing techniques, namely printing and coating. Since the polymers are processed in the liquid phase, usually as solution, printing techniques are a natural choice for applying and fixing a fluid in a structured way onto a flexible substrate. Essentially the printing process for functional polymer materials is identical to the printing of ink on paper and foils.

The process of printing polymer materials is a necessary condition for high productivity and low costs. A simple calculation visualizes this potential: a typical Si wafer production plant with a 30 cm wafer process has an annually processed area output of 88.000 m²/year. A typical printing machine, like a sheet feed offset printing press (1–3 m/s) or a web offset printing press (15 m/s) can produce the same area in 1–10 h. Given that the materials costs are low enough, the cost reduction due to printing techniques can be enormous for semiconductor processing. It is our opinion that printing techniques are the necessary tool for significant cost reduction for photovoltaics. Fig. 11 compares the efficiency of discrete, spin coated processed polymer solar cells and printed solar cells. It is observed that the average performance of printed solar cells is slightly below the average performance of discrete processed, spin coated solar cells, but the differences are small. With further emphasis on the improvement of processing techniques, especially with respect to the quality criteria for smooth, homogeneous layer structures with reasonable resolutions, printing techniques will certainly soon match the performance of discrete processing techniques. Under the assumption that the materials' prices (including packaging and substrates) will further fall with scale up, organic solar cells with a cost structure significantly below $1\text{€}/W_p$ can be realized.

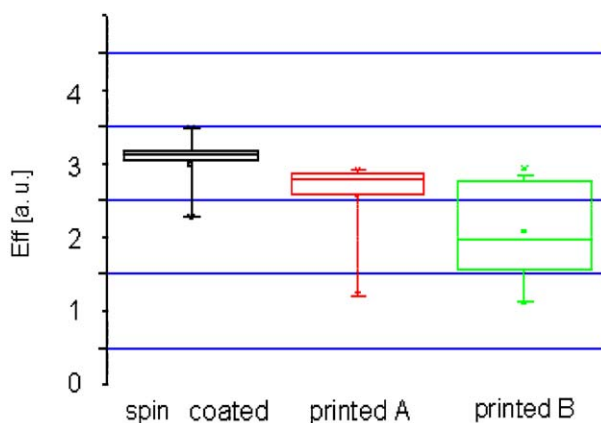


Fig. 11. Comparison of the efficiency of spin coated versus printed devices. The printed devices were produced in two batches, presented here as series A and series B. More than 30 devices were evaluated for each series and are presented in box plot diagram. The rectangular area in the boxplot diagram represents 75% of the devices, the highest and lowest values are marked by crosses.

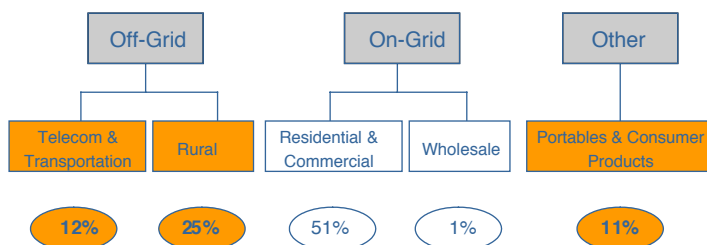


Fig. 12. Market segments of photovoltaics: approximately 50% of the produced solar cells are used in on-grid applications, where high efficiency and high lifetime are essential. The shaded market segments, especially rural and consumer electronics partially require a lower performance profile, making them more suitable for organic solar cells.

5. Conclusion

Fig. 12 summarizes the market opportunities for organic solar cells. There is still not enough experimental data to speculate on life times beyond + 5 years, which certainly would be necessary to enter the on-grid market. However, the market segments with more relaxed restrictions on the performance are significant as well and open enough possibilities for first applications. A necessary requirement for the market entry of these first applications is that organic solar cells show sufficient performance with respect to all criteria presented in Fig. 1. Most likely, the first applications will go into consumer electronics, indoor applications and novel, innovative applications. This may happen within the next 3 years.

References

- [1] S. Morita, A.A. Zakhidov, K. Yoshino, *Solid State Commun.* 82 (1992) 249.
- [2] J.J.M. Halls, C.A. Walsh, N.C. Greenham, E.A. Marseglia, R.H. Friend, S.C. Moratti, A.B. Holmes, *Nature* 376 (1995) 498.
- [3] G. Yu, J. Gao, J.C. Hummelen, F. Wudl, A.J. Heeger, *Science* 270 (1995) 1789.
- [4] N.S. Sariciftci, L. Smilowitz, A.J. Heeger, F. Wudl, *Science* 258 (1992) 1474.
- [5] S.E. Shaheen, C.J. Brabec, N.S. Sariciftci, F. Padinger, T. Fromherz, J.C. Hummelen, *Appl. Phys. Lett.* 78 (2001) 841.
- [6] P. Schilinsky, C. Waldauf, C.J. Brabec, *Appl. Phys. Lett.* 81 (2002) 1–3.
- [7] C.J. Brabec, S.E. Shaheen, C. Winder, N. Sariciftci, P. Denk, *Appl. Phys. Lett.* 80 (2002) 1.
- [8] F. Padinger, R. Rittberger, S. Sariciftci, *Adv. Funct. Mater.* 13 (2003) 85.
- [9] C. Waldauf, P. Schilinsky, J. Hauch, C.J. Brabec, *Thin Solid Films*, (2004), in print.
- [10] P. Schilinsky, M. Biele, C. Waldauf, C.J. Brabec (2004), submitted for publication.
- [11] P.M. Sommeling, et al., *Sol. Energy Mater. Sol. Cells* 62 (2000) 399–410.
- [12] I.D. Parker, *J. Appl. Phys* 75 (1994) 1656.
- [13] I.H. Campbell, T.W. Hagler, D.L. Smith, J.P. Ferraris, *Phys. Rev. Lett.* 76 (1996) 1900.
- [14] C.M. Heller, I.H. Campbell, *J. Appl. Phys.* 81 (1997) 3217.
- [15] C.J. Brabec, A. Cravino, T. Fromherz, N.S. Sariciftci, M. Minse, L. Sanchez, J.C. Hummelen, *Adv. Funct. Mater.* 11 (2001) 374.
- [16] D.R. Lide (Editor-in-Chief), *Handbook of Chemistry and Physics*, 75th Edition, CRC Press, Boca Raton, FL, 1995, pp. 12–113.
- [17] H. Frohne, S.E. Shaheen, C.J. Brabec, D.C. Müller, N.S. Sariciftci, K. Meerholz, *Chem. Phys. Chem.* 9 (2002) 795–799.
- [18] J. Yoon, J.-J. Kim, T.-W. Lee, O.-O. Park, *Appl. Phys. Lett.* 76 (2000) 2152.
- [19] T.M. Brown, R.H. Friend, I.S. Millard, D.J. Lacey, J.H. Burroughes, F. Cacialli, *Appl. Phys. Lett.* 77 (2000) 3096.
- [20] S.M. Sze, *Physics of Semiconductor Devices*, 2nd Edition, Wiley, New York, 1981.
- [21] S. Shaheen, C.J. Brabec, N.S. Sariciftci, G. Jabbour, *Mater Res. Soc. Symp. Proc.* 66 (2001) C.5.51.1-5.
- [22] J.J.M. Halls, K. Pickler, R.H. Friend, S.C. Morati, A.B. Holmes, *Appl. Phys. Lett.* 68 (1996) 3120–3122.
- [23] W. Geens, S.E. Shaheen, C.J. Brabec, J. Poortmans, N.S. Sariciftci, in: H. Kuzmany, J. Fink, M. Mehring, S. Roth (Eds.), *Electronic Properties of Novel Materials: Molecular Nanostructures*, Vol. 544, American Institute of Physics, New York, 2000, pp. 516–520.
- [24] R. Pacios, J. Nelson, D. Bradley, C.J. Brabec, *Appl. Phys. Lett.* 83 (2003) 4764–4766.
- [25] W. Geens, S.E. Shaheen, C.J. Brabec, J. Poortmans, N.S. Sariciftci, B. Wessling, *Org. Electron.* 3 (2002) 105–110.
- [26] P. Schilinsky, C. Waldauf, C.J. Brabec, *J. Appl. Phys.* (2004), in print.
- [27] P. Schilinsky, C. Waldauf, I. Riedel, V. Dyakonov, C.J. Brabec, *Adv. Mater.*, 2003, submitted for publication.